LEISA/Atmospheric Corrector (LAC) Validation Report

March 18, 2002

Dennis Reuter
NASA/GSFC
Code 693
Greenbelt, Maryland 20771

George McCabe
NASA/GSFC and Catholic University
Code 693
Greenbelt, Maryland 20771

NASA/GSFC

TABLE OF CONTENTS

LIST OF ILLUSTRATIONS AND TABLES

1.   INTRODUCTION

The LEISA (Linear Etalon Imaging Spectral Array) Atmospheric Corrector (LAC or AC) on Earth Observing-1 (EO-1) is a hyperspectral imager providing 256-channel continuous spectra in the wavelength range from 0.89 to 1.58 microns. It has a single pixel spatial resolution of 250 meters, a 185-km swath-width and a spectral resolving power ($\lambda/\Delta\lambda$) of 150 or greater ($\Delta\lambda < 10$ nm) throughout its spectral range. The imager employs a wedged filter, a sophisticated 2-dimensional filter whose transmission wavelength varies along one of the dimensions to provide its spectral resolution. The use of the wedged filter greatly simplifies the optical/mechanical design, so that the instrument is adaptable to a wide variety of platforms (i.e., it is a "bolt on" imager).

This paper presents an overview of the camera that highlights its unique features from both a design and data standpoint. It discusses the pre-launch instrument characterization process and on-orbit performance. This includes the use of solar and lunar calibration techniques to obtain absolute radiometric calibration. The application of the data to the problem of atmospheric correction of high-spatial resolution multi-spectral satellite images (e.g., Landsat-type) is also discussed.

A problem common to all measurements obtained by high-spatial resolution multispectral (MS) imagers aboard satellites is the systematic errors in the apparent surface reflectances caused by atmospheric effects. Temporal and spatial variability in atmospheric scattering and absorption due to aerosols, clouds and molecular species, primarily water vapor, must be accounted for in the retrieval of accurate surface properties. The research team has developed the high spectral/moderate spatial resolution wedged filter hyperspectral (HS) imager, the LAC, to correct high-spatial, low-spectral resolution MS imagery for atmospheric effects. The spectra it provides may be used to correct images from the Advanced Land Imager (ALI) on EO-1. Because EO-1 is flying in formation one minute behind Landsat 7, the data may be used to correct Landsat 7 also. The LAC provides scientific return both in terms of improved imagery and moderate spatial resolution hyperspectral sensing capabilities. It advances three technologies that are relevant to a number of remote sensing applications. These are listed as the first three items in the introduction to Section 3. TECHNOLOGY VALIDATION.

2.   TECHNOLOGY DESCRIPTION

The LAC employs a state-of-the-art wedged infrared (IR) filter (a linear variable etalon or LVE) placed very close to a two-dimensional IR detector array to produce a 2-D spatial image that varies in wavelength along one of the array dimensions. (The LVE is a wedged dielectric film etalon whose transmission wavelength varies along one dimension.) The filter has a nearly linear dependence of wavenumber on position. It has a 0.45-cm section which covers the 1.2- μm to-1.6-μm spectral region at a resolution of ~35 cm^{-1}, and a 0.55-cm section covering the 0.9-to-1.2-μm spectral range at a resolution of ~55 cm^{-1}. The sections are bonded together to form a single filter assembly. This filter represents an advance in dielectric thin film technology. Reflective 1/4-wave stacked layers placed on both sides of a 1/2 -wave etalon cavity provide the spectral resolution. Out-of-band suppression of the etalon is accomplished with lower resolution filter layers. The wavelength transmitted by all the layers varies as a function of position, thus providing the spectral information.

The two-dimensional spatial image is formed on the array by a small, wide field of view (WFOV) lens. The filter is mounted within 200 μm of the array, so the image is formed simultaneously on the array and the filter. The spectrum of each point of the area imaged is obtained as the orbital motion of the spacecraft scans the image of that area along the focal plane in the variable wavelength dimension. This creates a

three-dimensional spectral cube. The spatial resolution is determined by the angular resolution of the imaging optic, the image scan speed and the readout rate of the array. The LAC has a single pixel spatial resolution of 360 µradian x 360 µradian corresponding to a single pixel FOV of 250 m x 250 m for a 705 km orbit. The LAC uses three identical subassemblies in a single module to match the Landsat 7 swath width of 185 km (~15°). Each subassembly consists of a focal plane formed of a wedged filter mounted to a 256 x 256 pixel indium gallium arsenide (InGaAs) detector array placed behind a lens covering a 5° x 5° FOV. The InGaAs detector material was fabricated by Sensors Unlimited of Princeton New Jersey, and was hybridized to a TCM 2620 multiplexer by the Boeing (Rockwell) Science Center in Thousand Oaks, California. The middle lens is used on-axis while the other two lenses are used off-axis to cover the full 15°. So each off-axis lens must have a usable 15° x 5° FOV. Thus a single frame consists of an effective focal plane with 768 pixels in the cross-track direction and 256 pixels in the along-track direction. A frame readout rate of approximately 28 Hz matches the image motion caused by the orbital velocity to the interpixel angular separation. That is, the orbital motion of the spacecraft moves the image 1 row in ~0.0356 second. The wedged filter design was chosen for its optical and mechanical simplicity compared to conventional grating, prism, or Fourier transform spectrometers tunable filter systems. As discussed below, this method of obtaining spectra does place some stability constraints on the spacecraft and the scene. The LEISA concept was originally developed at NASA Goddard Space Flight Center (GSFC) under the Advanced Technology Insertion Program for the Pluto Fast Flyby Mission [1]. The filters were designed and fabricated by the Optical Coating Laboratories Inc. of Santa Rosa, California, with the aid of test results obtained at NASA (GSFC) [2,3]. The wedged filter concept has also been developed independently at Hughes Santa Barbara Research Center [4] and their Wedged Imaging Spectrometer (WIS) operating in the visible and near-IR (VNIR) regions has been demonstrated in aircraft flights [5].

The LAC is composed of two modules, the optics module and the electronics module. Figure 1 shows both modules being tested in the laboratory. The optics module contains the lenses, focal planes, and electronics necessary to operate the arrays and to transfer the digitized pixel data to the electronics module. It is mounted to the nadir deck of the spacecraft and bore sighted with the ALI. The electronics module contains the command and data interface to the spacecraft, the array timing and bias circuitry, the thermal electric cooler (TEC) control circuitry, and the instrument power supply. It is mounted in a bay below the nadir deck. Because the long-wavelength cut-off of the arrays is 1.6 µm, they may be operated at near room temperature. However, to decrease the dark current and increase the signal-to-noise ratio, TECs are used to stabilize the array temperatures at ≤285K.
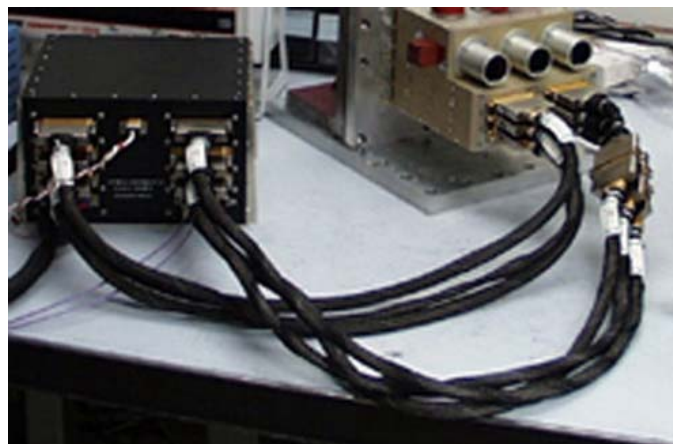
Figure 1. LAC electronics module (left) and optics module. The three lenses are facing outward. The electronic module is 25 cm x 23 cm x 18 cm. The optics module is 19 cm x 18 cm x 14 cm. The cable is separated into two groups of three, one group carrying the analog signals and biases, the other carrying the clock signals.

Figure 2 shows a view of the optics module as it is oriented on the nadir deck. In normal operation the lenses would be facing earthward while the solar calibration tubes would be facing along the direction of the spacecraft motion. During a solar calibration the solar calibration tubes are pointed to within 1° of the sun, and light entering the tubes is reflected off a small spectralon target, providing a reproducible illumination pattern across the focal planes. Because the sun is not imaged through the lenses, it provides only an approximate absolute radiometric calibration. In flight radiometric calibration is provided by lunar scans and by comparisons with the other instruments on EO-1 (ALI and Hyperion). Several well-instrumented ground sites are also used for radiometric calibration. Figure 3 shows the interior detail of the optics module. In normal operation, light comes from the right through the triplet lens and is imaged onto the focal planes at the left. The cylinder directly above the focal plane is a stray light baffle. The baffles in the solar calibrators are evident, as is the spectralon reflector. Note that there are three electronics boards, one for each focal plane. The far-left side is mounted to the nadir deck and the TEC heat sinks are mounted to this side. The use of a two-module design for the LAC allows a greater degree of flexibility than using a single module. Optical modifications (e.g., wavelength range, resolution, etc.) require changes only to the optics module while spacecraft interface changes (e.g., command and data handling (C&DH), power levels, etc.) require changes only to the electronics module.
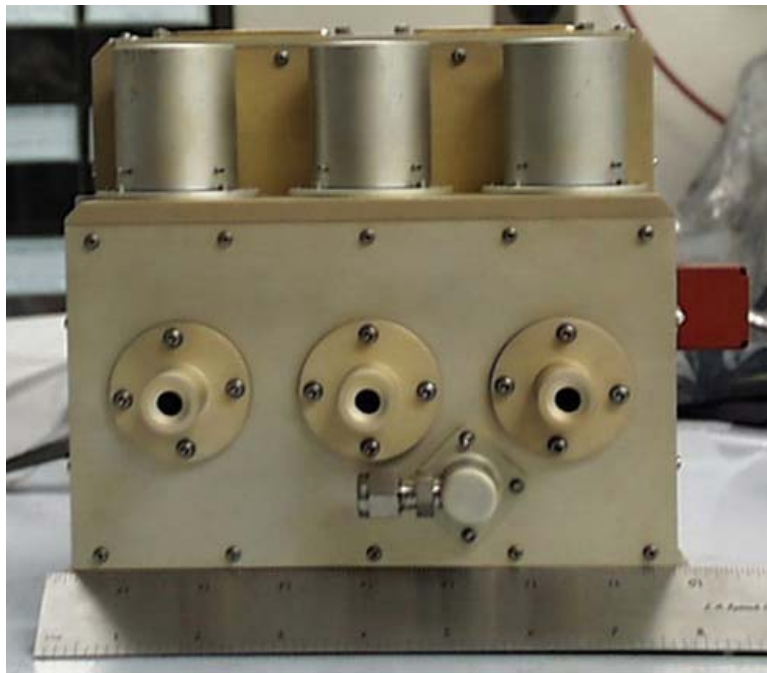
Figure 2. Optics module with lenses facing upward and solar calibration tubes facing forward. The red object to the right is a cover for the optical alignment cube used to align the LAC with the ALI. The fitting in front is an N$_2$ purge coupling used before launch.
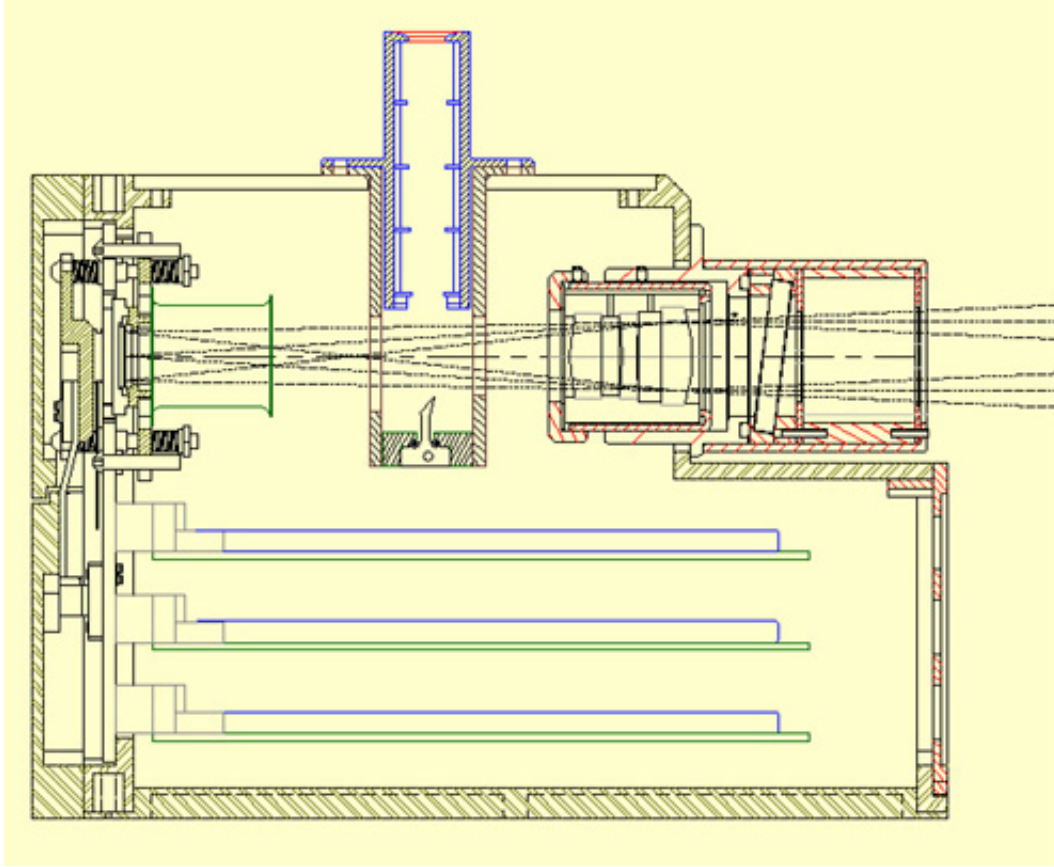
Figure 3. Optics module details. The array/LVE assembly is to the left while light from the scene enters to the right through an anti-reflective (AR) triplet lens. The spectralon target for the solar calibrations is at a 45° angle. The target is sized to approximate a 30% reflectance surface at 60° solar angle. The tilted element before the lens is a visible/UV reflector.

The LAC has a total mass of 10.5 kg: 4.4 kg for the electronics module, 3.9 kg for the optics module, and 2.2 kg for the cable connecting them. It uses a maximum power of 45 W on start-up, which decreases to about 35 W for a TEC temperature setting of 275 K, once the temperature is stabilized. At the nominal fame rate of 28 Hz, which slightly oversamples the spatial dimension in the along-track dimension, the data rate is 95 Mbits/s (12-bit analog-to-digital (A/D) converters are used). A frame rate of 56 Hz allows double sampling in the along-track spatial dimension at the expense of reduced single-frame signal-to-noise ratios (SNRs). The LAC frame rate could have been adjusted to provide exact single sampling as was done for ALI, however, for simplicity this was not done.

A significant difference between push broom filter imagers such as LAC and ALI and slit imagers such as Hyperion is in the way spectra are formed. In an LVE camera an image is obtained, however, several images are required to complete the spectrum of a given point in the scene. Thus, excess drift in the image motion can cause a point to cross columns during the acquisition of a full spectrum (see [6] for a discussion of re-sampling in wedged filter spectrometers). Control and knowledge of the EO-1 spacecraft, and the alignment of the LAC along-track axis to the ALI along-track axis to within 2 arc-minutes, limits this uncertainty to a fraction of a pixel. In the worst case, across-track drift and along-track timing errors lower the effective spatial resolution to 2 pixels, or the Nyquist sampled spatial resolution. In comparison, slit-type imagers obtain all the spectral elements of a given point on the surface simultaneously. In

practice, however, off-axis image errors, as well as the effect of oblique incidence for gratings and non-linearity effects for prisms, cause the spectrum to be tilted and/or curved in the focal plane, and thus not to track along a column. These geometric effects are the analog of imperfect sampling in the wedged filter camera, and also cause a loss of effective spatial resolution. A wedged filter camera is inefficient for small sources (e.g., to obtain the spectrum of a point source), but it is essentially as efficient as a slit-type instrument for extended sources (e.g., images of the earth's surface from a near earth orbiter). The instrument characteristics of the LAC are summarized in Table 1.

Table 1. Instrument Summary

Type of Spectrometer: Wedged Filter

Spectral Coverage: 0.89 to 1.58 µm continuous (SNR>10, 0.94 to 1.58 µm)

Spectral Resolving Power: ~35 cm^{-1} ($\Delta\lambda$: 5 nm @ 1.2 µm, 9 nm @ 1.6 µm)

  ~55 cm^{-1} ($\Delta\lambda$: 4 nm @ 0.9 µm, 8 nm @ 1.2 µm)

Wavelength Dependence: Linear in Wavenumber ($\Delta\lambda^{-1}$)

Imaging Optics: Three Multi-Element Refractive, 15° FOV Lenses (f/8, 11.4 cm focal length)

Dynamic Range: 2048

Frame Rate: Nominal 27.8 Hz, Maximum 55.6 Hz

Single Pixel FOV: 0.36 x 0.36 mrad^2 (250 x 250 m^2 for 705 km orbit)

Three Array FOV: 264 x 92 mrad^2 (185 x 64 km^2 for 705 km orbit)

Memory Required for One 185 x 64 km^2 Spectral Map: 810 Mbits

Data Rate: Nominal, 95 Mbits/sec; Maximum, 190 Mbits/sec

Arrays: 256 x 256 PV InGaAs, 40 µm pixels (TCM 2620 Multiplexer)

Selectable Focal Plane Temperatures: ~ 285 K, 280 K, 275 K, 265 K

Power: 48 W peak; 35 W nominal, <10 W orbit average (maximum 20% duty cycle)

Mass: 10.5 kg

  Electronics Module (1773 Interface, Power, RS 422 Data Interface, Array Control): 4.4 kg

  Optics Module (Optics, Arrays, Solar Calibrators, TECs, Amplifiers, A/D): 3.9 kg

  Inter-module Cable 2.2 kg

3. TECHNOLOGY VALIDATION

The primary purpose of the LAC on EO-1 from an orbiting technology validation standpoint is fourfold: 1) to validate the use of the wedged filter method for obtaining hyperspectral images, 2) to validate the use of a multi-array, multi-telescope system to synthesize a wide-field imager, 3) to validate the use of non-cryogenic InGaAs IR arrays for moderate resolution spectroscopy and, 4) to validate the use of lunar and solar measurements (in conjunction with ground-based measurement campaigns) to provide calibration. The science validation is to provide a demonstration of the ability of moderate-spatial resolution hyperspectral measurements to provide real-time atmospheric correction information to high-spatial resolution multispectral sounders. This report will not deal with the scientific validation issues.

3.1 Ground Test Verification
Prior to launch, the operational characteristics of the LAC, including dark current, read noise, radiometric sensitivity, central wavelength, bandwidth and angular position, were measured for each pixel. The low-illumination noise limit (read noise + dark current) were about 1 – 2 counts. While near saturation, in the photon noise limited regime, SNRs of several hundred were obtained. The overall photon to photoelectron conversion efficiency ranged from 0.10 to 0.20. For the most part the characteristics measured prior to

launch have not changed with two exceptions: the number of non-responsive pixels has increased since launch, and a systematic noise source not apparent in pre-launch tests, and therefore presumably occurring after launch, has modified the radiometric calibration. These effects will be discussed in the next section.

The pre-launch spectral characteristics of each pixel were measured using a grating monochrometer whose resolution was much higher than that of the wedged filters. A white light source was imaged onto the entrance slit of the spectrometer and a grating blazed for 12 μm was used to disperse the light. Thus at each grating setting several orders would be present simultaneously, for example, at a 12-μm setting light in orders 13 thru 8 would fall into the 0.92 to 1.6-μm range. The output slit of the monochrometer was placed near the focal point of each lens of the LAC, filling each array with collimated light in 5 to 7 orders. Thus, at each grating setting, light would be transmitted at several rows of the array. The central wavelength and bandwidth of each pixel were determined by stepping the grating in small (1 to 5 nm) increments and fitting the resultant intensity vs. wavelength data to a Gaussian function. Examples of these fittings are shown in Figure 4. As may be seen from this figure, the resolving power of the filter is quite high (e.g., > 200 at 1 μm).
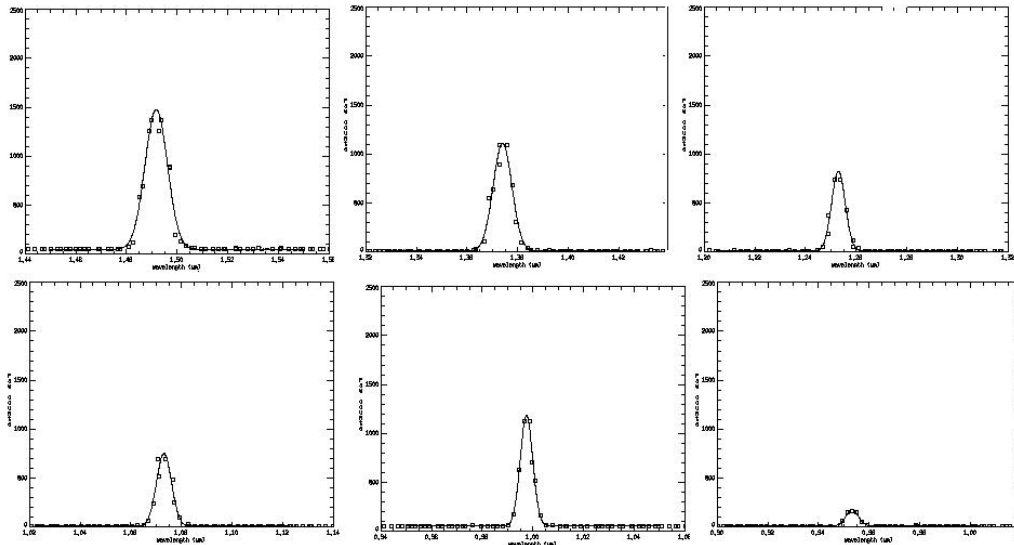
Figure 4. Examples of spectral line-shapes measured with the monochrometer system. A Gaussian line-shape was fitted.

In fact, the spectral line-shape at each pixel is closely described by a Gaussian function whose full-width at half maximum is 53.34 cm^{-1} for the short-wave filter segment (0.89 to 1.23 μm) and 36.84 cm^{-1} for the long-wave segment (1.21 to 1.58 μm). Figure 5 summarizes the results of fitting Gaussian functions with a single width to normalized intensity vs. wavenumber measurements for several pixels in each filter segment. The wavenumber of each pixel depends nearly linearly on row number.

6
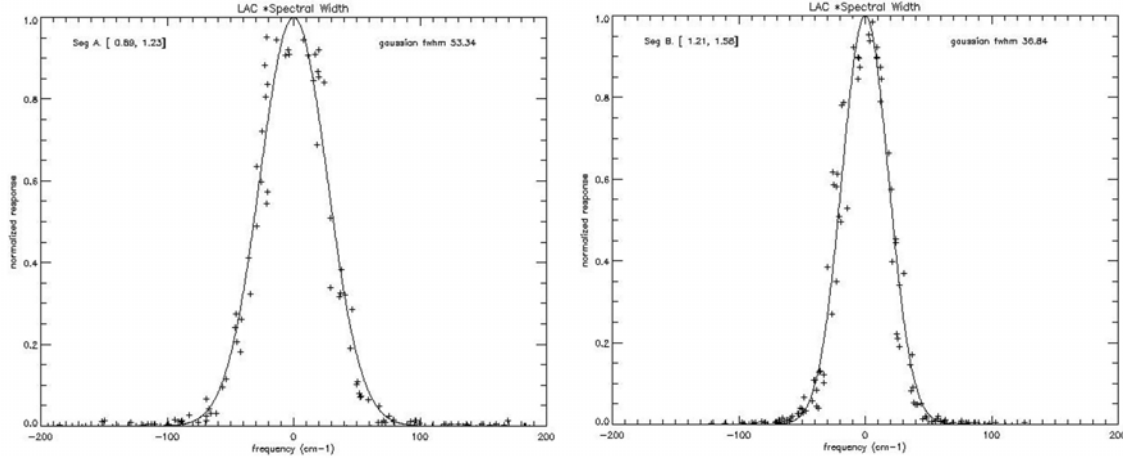
Figure 5. Summary of fittings of measured normalized pixel responses to a single Gaussian function (width in wavenumbers) for the short-(left panel) and long-wavelength filter segments. Pixels covering the entire spectral range are included in the fittings. The constant width in cm^{-1} is consistent with a linear dependence of wavenumber with position on the filter.

The angular positions of each pixel in each array were determined relative to an alignment cube attached to the surface of the optics module prior to launch. The measurement was performed using two theodolites. One theodolite was aligned with the surfaces of the cube and used as a transfer standard to determine the angular displacements of the second theodolite. The second theodolite was equipped with a cross-hair target at the focal point of a lens simulating a source at infinity. When re-imaged by the lenses of the LAC, an image of the crosshair was formed on each of the focal planes. The image of the crosshair was ~20 pixels across, allowing the center of the crosshair to be located to ~0.1 pixel. The image of the crosshair was translated along the nominal along-track direction of each focal plane by rotating the theodolite source. Position measurements were made at several locations for several rows of each array. In this way, the roll and yaw angles of each array were determined to approximately 40-microradian accuracy (0.1 pixel). This information was used to map the angular position of each pixel for use in geolocating the on-orbit image data. These data were also used to mount the LAC to the nadir deck of the spacecraft in such a way that the yaw angle of the LAC array that overlaps the field-of-view of the ALI was parallel to the ALI yaw angle to within 1 arc-minute. This ensured that there was minimal across-track drift (< 0.25 pixel) during a scan.

3.2   On-Orbit Test Validation

 On-orbit validation includes: 1) determining the stability of the arrays under conditions of no illumination, 2) determining the instrumental noise characteristics under conditions of illumination, 3) determining the image quality, 4) determining the absolute radiometric calibration accuracy, 5) assessing the ability to obtain spectra and 6) co-locating LAC images with Landsat 7 images. A typical on-orbit data collection event (DCE) lasts about 40 seconds during which ~1100 frames are obtained at the 28-Hz frame rate (2200 at 56 Hz) and produces a complete spectral image over an area of ~210 km x 185 km. The operation of the instrument is extremely simple. Power is applied to the instrument about 9 minutes before image data is taken to insure the array temperatures and electronics have stabilized. The frame rate, array temperature set-point and array sensitivity are set by issuing three commands. The data clock is enabled about 8 seconds before the instrument is pointed at the desired surface location to insure that all spectral bands are obtained for the entire target area.

3.2.1 Dark Current Stability

The LAC dark current is measured within 1 orbit of a DCE by imaging a region on the unlit hemisphere of the earth's surface for 1 second (a dark DCE). The average of these dark data is subtracted from each frame of the DCE to remove offsets and dark current at each pixel. The subtraction is done as part of the ground processing of the data. The dark current is very uniform during a dark DCE, with the frame-to-frame standard deviation of each pixel typically being less than 1 count. The dark current is also very stable from day to day, with only a slight drift apparent. This is illustrated in Figure 6, which shows histograms of the differences between a dark DCE on day 198 of 2001 (July 17, 2001) and two previous dark DCEs (February 27, 2001 and April 30, 2001). From this figure one can see that there is a general broadening of the dark current difference distribution over long periods of time (i.e. weeks) and there appears to be a tendency for the dark current to increase slowly as a function of time. The final panel in the figure shows the reproducibility of the offset on a single day, which is indicative of the error in the offset subtraction methodology. This error of somewhat less than 1 count is the limiting error in the low illumination case. The bias of 0.5 count in the last panel is representative of the array temperature control stability.
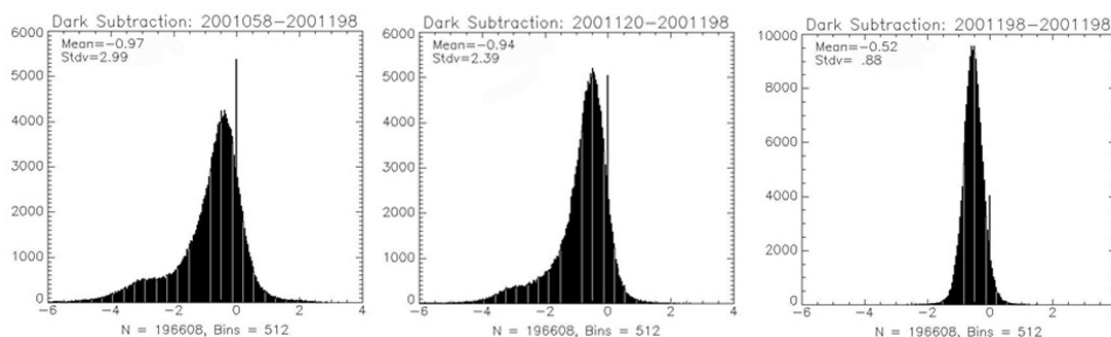
Figure 6. Histogram of difference between a dark DCE on July 17, 2001 and dark DCEs February 27, 2001 (leftmost panel), April 30, 2001 (center) and a separate dark DCE on July 17, 2001. Note the tail of the distribution indicating a slight increase in dark current as a function of time. The rightmost panel shows the difference for two dark DCEs on July 17, 2001.

The slow broadening of the dark current distribution is probably related to an observed slight increase in non-responsive pixels since launch. At launch there were about 400 non-responsive pixels (~0.2% of the total) and in the 8 months since then another 1100 have been added (for a total of ~0.8%). Typically this number grows at a rate of one per day, however on two occasions several hundred pixels have "died" within a single DCE. (Note: Since the instrument is turned off between DCEs it is possible the pixel mortality could have occurred at any time since the turn-off after the previous DCE and the beginning of data at the current DCE). There were no other operational (e.g. radiation, solar cell overvoltage, etc.) or instrumental (e.g., overvoltage, excess current, etc.) anomalies at these times and the cause of the increased non-responsive pixels is still being investigated. It has had no major operational effect since the relative number of pixels affected is still quite small (<1%) and they are scattered throughout the arrays. Prior to launch the arrays were damaged by contact with the wedged filter holders during a vibration test. The contact was caused by an incorrect assembly procedure that was subsequently corrected and no further damage was observed in additional vibration testing. However, gradual long-term effects on the multiplexer bump bonds from this incident remains a strong candidate for the cause of the pixel mortality.

3.2.2 Illumination Noise Characteristics

The limit on the SNR under most illumination conditions is determined by the Poisson distributed statistical variance of the photon flux from the source. The solar calibration DCEs are used to evaluate this limit for the LAC, since the illumination is constant. The standard deviation of each pixel is measured

over the 200 frames obtained during the calibration and the ratio of this to the average signal is used to determine the SNR. Figure 7 shows a wavelength dependent summary of the SNR obtained in this fashion. The discontinuity at ~1.2 μm marks the boundary between the two filter segments. Note that the SNR is greater than 100 everywhere, consistent with pre-launch calculations. In fact, since the solar calibration level is only about 25% of the maximum before saturation is reached, the maximum SNR is expected to be about a factor of 2 higher than shown here. However, as discussed below, a systematic noise source that apparently occurred after launch limits the actual SNR to values lower than shown in Figure 7. Since digital saturation occurs well before the actual analog detector saturation (digital saturation occurs at about 20% of the 2.5 million electron detector element full well), the signals do not show large non-linearities near saturation.
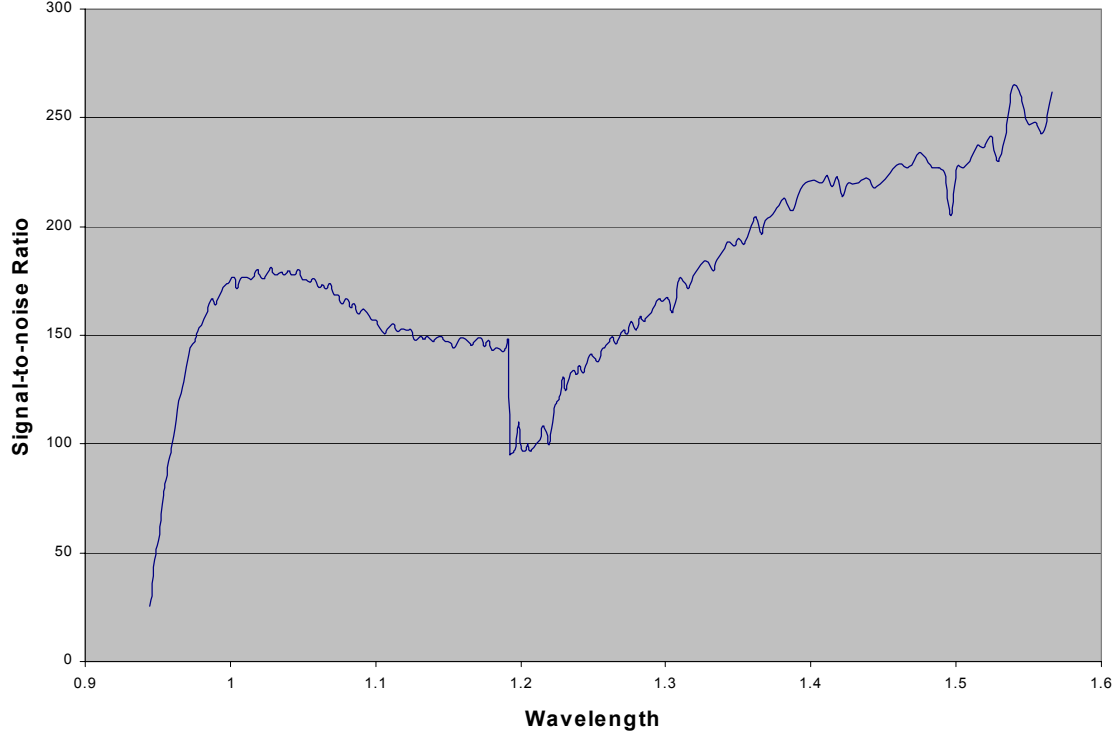
Figure 7. SNR as a function of wavelength determined from a sole calibration DCE in the method described in the text. The rapid drop-off at wavelengths shorter than 0.97 μm is caused by loss of quantum efficiency in the InGaAs arrays.

As mentioned above, the actual LAC noise is dominated by a systematic source that appeared after launch. Initially, it was very difficult to obtain images not showing excessive pixel-to-pixel variation (streaking) at nearly the 10% level. The source of this streaking was found only after a scanning solar calibration showed that for most illumination levels there was a relatively constant "fixed pattern" noise that did not appear in the dark frames. In a scanning solar calibration, the solar calibration tubes are nodded ± 6° about the solar direction, thus varying the amount of light scattered off the spectralon target in a non-calibrated but uniform way. This maneuver was initially performed to assess the stability of illumination during a solar calibration, and not as an additional calibration method. Figure 8 shows a plot of a typical row of all three arrays for several positions of the solar calibration tubes.

9
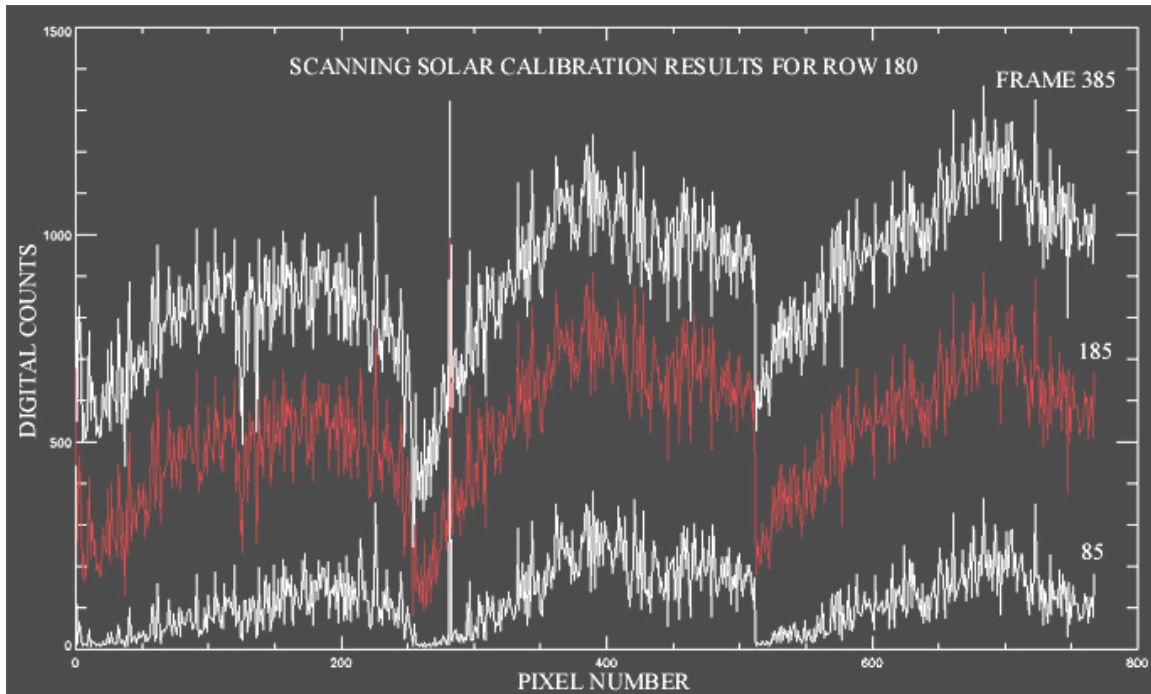
Figure 8. Plot of row 180 for all three arrays showing the "fixed pattern" noise. As the pointing of the solar calibration tubes is rolled about the solar position, the array illumination varies from a maximum in frame 385.

The offset has been subtracted in this plot. Two observations immediately present themselves: 1) for most illumination levels there is a large, relatively illumination independent pixel-to-pixel variation which 2) does not decrease the number of counts below the dark level (i.e., there are no large negative numbers in the differences). Data from the scanning solar calibrations are now used in the calibration method to account for this "fixed pattern" noise. That it is very reproducible for a given illumination level is evidenced by the nearly photon-noise-limited variance of the signal from any given pixel during a non-scanning solar DCE (e.g., Figure 7). Unfortunately, one irreversible effect of this noise is that once the resultant of the illumination and the noise combines to give the same output count as the offset level, further reductions in illumination do not lower the output level. Thus, there are uncorrectable non-linearities at low illumination levels. Prior to launch, the only time all spacecraft systems could be operated was during thermal vacuum testing and the "fixed pattern" noise was not seen in LAC data from the last illuminated test carried out at that time. Since subsequent LAC tests were carried out in non-illuminated conditions, all that may be said is that this noise appeared sometime between the last thermal vacuum test and the first on-orbit DCE. The most likely causes of this systematic noise component are: 1) although the thermal-vacuum tests were designed to closely simulate orbital conditions it is possible that there is a system interference that was not present in these simulations, 2) launch vibration could have altered the LAC and, 3) power supply filter components that were stressed by an overvoltage condition during the conducted susceptibility test may have failed. The causes are still being investigated.

3.2.3 Image Quality

Prior to launch, the image quality was checked by imaging a simulated source at infinity onto a single pixel. The on-orbit terrestrial surface images indicate that the focus has remained good after launch. As a further test, images of the Moon obtained during the lunar calibration scans have been used to determine the rise distance of a sharp boundary. The results, as illustrated in Figure 9, show a rise from 5%

illumination to 95% illumination in approximately 1 pixel, again indicating excellent focus and image quality.
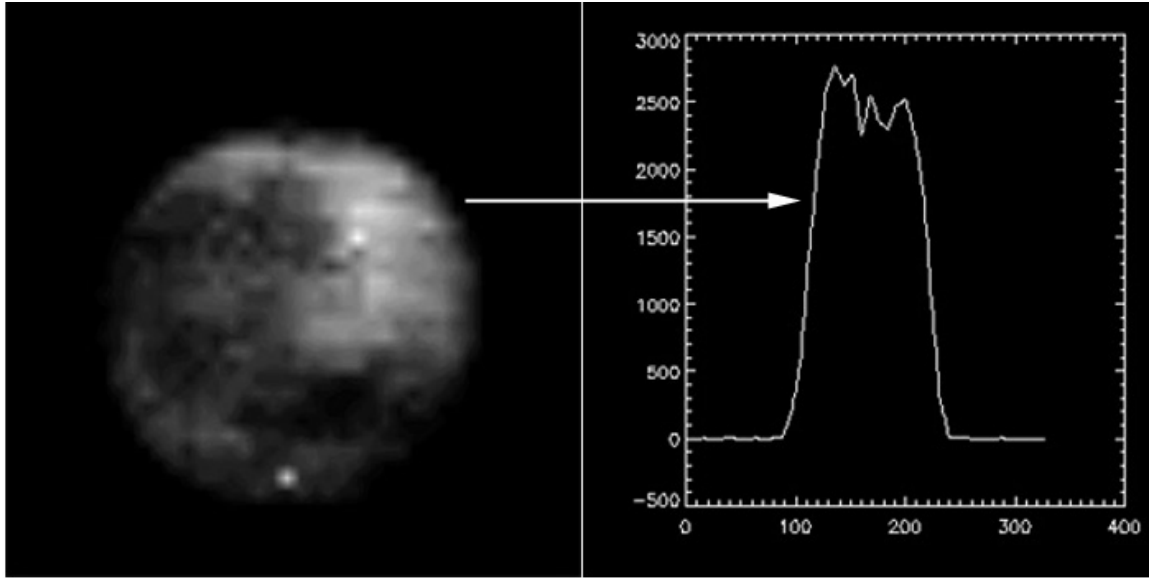
Figure 9. Lunar image (expanded by a factor of 8) showing rise and fall distances (5% to 95%) of 8 to 10 pixels (on expanded scale), indicating single pixel imaging capability. Without expansion the moon fills about 20% of an array (~25 pixels).

3.2.4   *Out-of-band Transmittance*

A concern frequently raised about wedged filter spectral imagers is that there may be excessive out-of-band spectral transmittance. If this were significant, then flux measurements at any wavelength would be contaminated by the flux at all other wavelengths in a complex manner. LAC solar calibration measurements show that the integrated effect of out-of-band transmittance is less than 1%. This is illustrated in figure 10, which shows a plot of the relative response of the LAC, averaged over all three arrays, as a function of λ for wavelengths near the InGaAs response cut-off. The sharp cut-off at wavelengths less than 1 μm follows the curve expected for these back-illuminated arrays. For wavelengths where the in-band transmission maximum is less than ~0.93μm, the maximum signal is always less than 1% of the available in-band flux because the detector elements are not sensitive to these short wavelengths. If there were significant out-of-band transmittance, wavelengths longer than the array cut-off would impinge on the detectors, which would give rise to a signal.

11
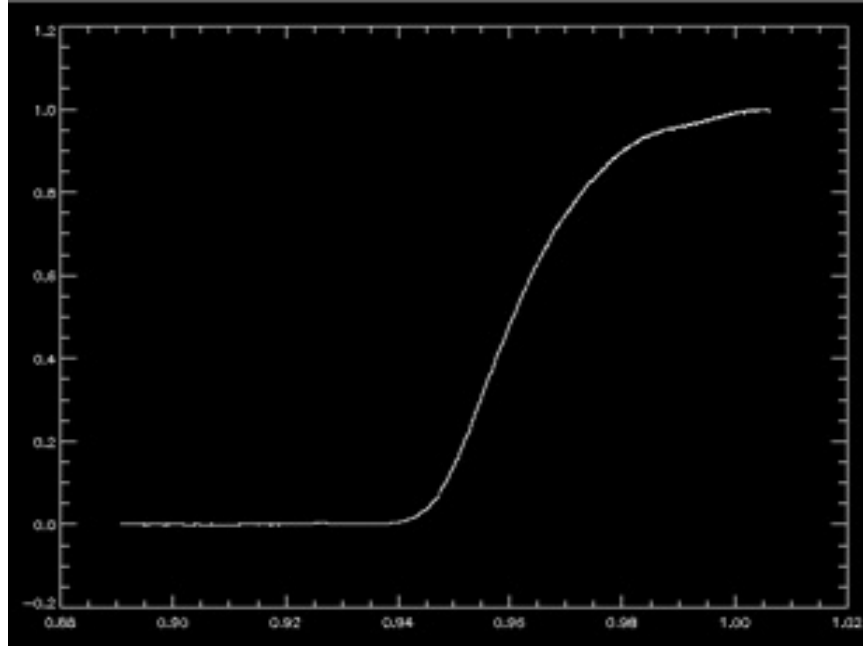
Figure 10. Relative shortwave response for LAC solar calibration. The lack of signal at wavelengths less than 0.93 μm indicates that there is little out-of-band filter transmittance.

3.2.5 Absolute Radiometric Calibration and Spectra

Because of the relatively recent identification of the "fixed pattern" noise in the images, the absolute radiometric calibration is still proceeding. The ability to create spectra is illustrated in Figure 11, which shows two spectra obtained in regions near the Suez Canal. The differing water vapor absorption is clearly visible here.
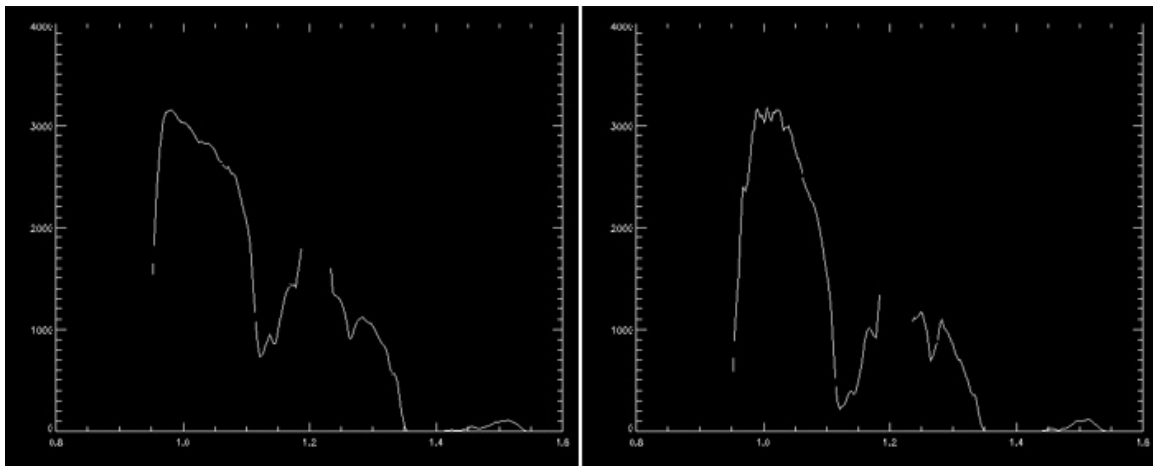
Figure 11. Two spectra obtained in different regions near the Suez Canal. Note the much deeper absorption at 1.13 μm in the right panel, indicative of greater atmospheric water vapor.

3.2.6 Co-location With Landsat 7

As part of the data processing, single wavelength LAC spectral images are placed on a latitude-longitude grid for comparison with Landsat 7 multispectral data. This involves two steps: 1) using the complete pixel by pixel central wavelength map described in Section 3.1, pixels within ½ resolution element of a desired wavelength are selected and also the angular position of these pixels is taken from the position map described in Section 3.1; and 2) the angular positions are projected onto a surface latitude-longitude map using the spacecraft attitude information provided as part of the ancillary data on each data tape. As shown in Figure 12, this process produces accurately positioned maps, further verifying the pre-launch angular measurements. The potential utility of the LAC for correcting Landsat 7 data is illustrated here, since the real-time atmospheric features are the same in both data sets.
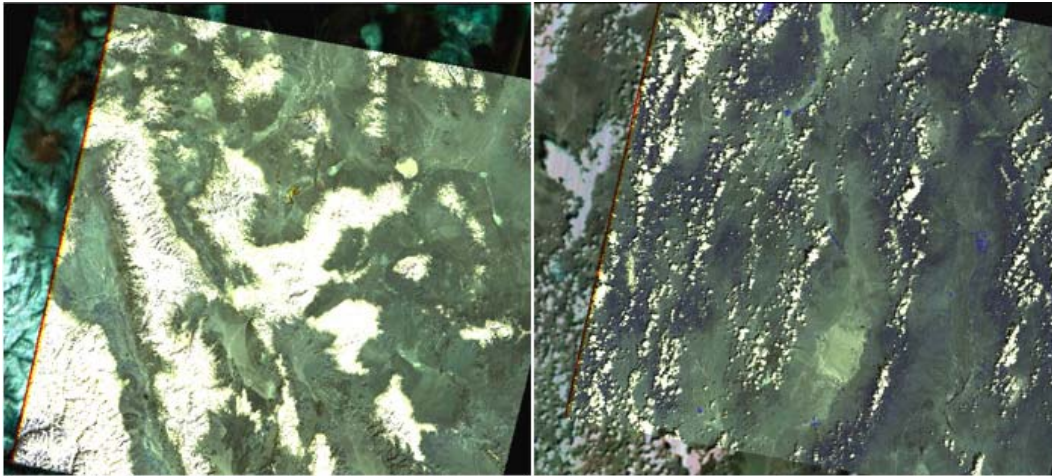
Figure 12. Overlay of Landsat 7 image on LAC image taken within 1 minute. Railroad Valley, Nevada (left) and Cuprite, California (right) are used as calibration areas for these instruments. The features in the images are well correlated.

3.3   On-Orbit Usage Experience

As of this writing, the LAC has obtained approximately 1600 DCEs without any instrument failures. As shown diagrammatically in Figure 13, Level 0 image data is received from the GSFC Data Processing Facility (DPF) on tape media and processed to Level 1R (radiometrically calibrated) data at the LAC DPF.
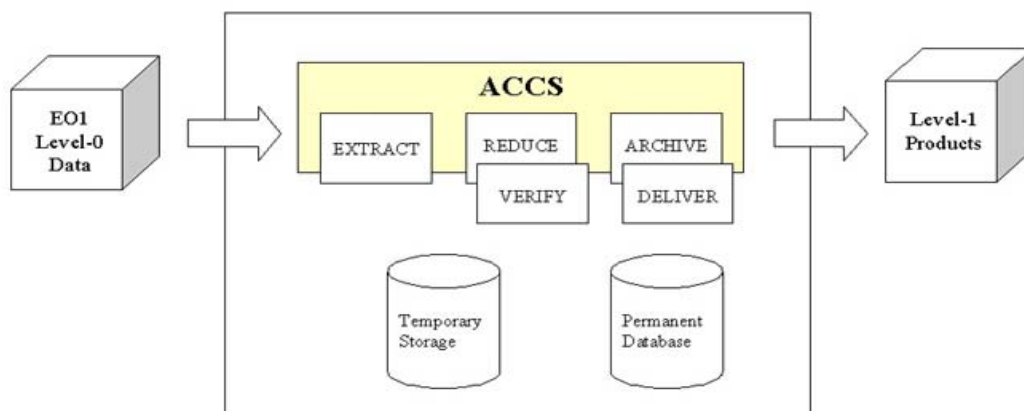
Figure 13. Schematic of EO-1 LAC data flow. ACCS (Atmospheric Corrector Calibration System).

More highly processed data sets, such as the geo-located data sets, are done on an as needed basis and require more computation time. These processes are currently being automated as well. Data is provided to researchers as requested through the GSFC Science Validation Facility (SVF). Currently, research requests through the EO-1 science validation NASA Research Announcement (NRA) are supported.

To correct for the "fixed pattern" noise an extended calibration procedure was created for the ACCS. The standard offset and scale calculation for converting raw values to radiometrically calibrated ones is exchanged for a discreet look-up-table (LUT) approach. The LUT is an indexed array that contains a scaled value for every raw value within the dynamic range of the system. Solar scanning and staring DCEs are used in generating the calibration dataset. Direct solar irradiance, not modified by the earth's atmosphere, may be detected through the calibration inputs of the LAC, designed specifically for this purpose. Light passing through a calibration port is uniformly scattered by a Spectralon surface onto the image plane. In scanning solar DCEs the average transmission of sunlight through the calibration inputs varies with illumination angle, and all levels from 0 to 100% are recorded during rotation of the spacecraft around an axis perpendicular to the line of site. The relative response of each detector pixel to uniform illumination may be determined in this way. Staring solar scans may be used to refine the estimates of pixel response at the corresponding input level. The individual response "functions" of the LUT represent corrections of each pixel relative to one or a group of "master" pixels. Absolute radiometric correction of detector response is achieved by rescaling LUT values according to the ratio of response of master pixel(s) values in lunar calibration scans to the U.S. Geologic Survey (USGS) model of moon intensity [Keifer, private communication, 2002]. Intercomparisons of LAC data for Earth scenes with ground truth measurements, and data from independently calibrated sensors (Hyperion) may be used to verify/refine the first stage correction.

The ACCS extended calibration procedure may be briefly summarized as follows. Reducing solar scan data to numbers for the calibration LUT is an automatic process, nevertheless it is time consuming. The pertinent frame subset of the solar scan is selected. Spurious noise is filtered from each pixel scan profile. The location and value of the peak of the profile is estimated by a low order fit function. The ratio of response relative to the master pixel(s) for each input level is saved in a binary file, the calibration LUT, where each column-row layer of the 3 dimensional array corresponds to a single input level. The relative scale of LUT response "functions" is refined with staring solar DCE data. The result of the LUT procedure is a reduction of the systematic error in the calibrated result to 5%. Converting Level-0 data to Level-1R is computer-resources intensive and can take four times as long as the standard calibration procedure. To conserve disk space and maximize access speed, values are stored as 16 bit integers with a real type-scaling factor for translating to radiometric units. For the correction subprocedure, input levels are indexed to relate pixel values to directly array elements. In other words, The LUT is constructed such that raw integer counts identify the location of calibrated values in the result. Typically, the calibration file must be accessed randomly 10^8 times in converting a Level-0 dataset to Level-1R. A caching algorithm planned for the next release of the ACCS software will improve performance significantly.

Figure 14 illustrates the improvement in uniformity gained by using the LUT obtained in two steps from the scanning and fixed solar calibrations.
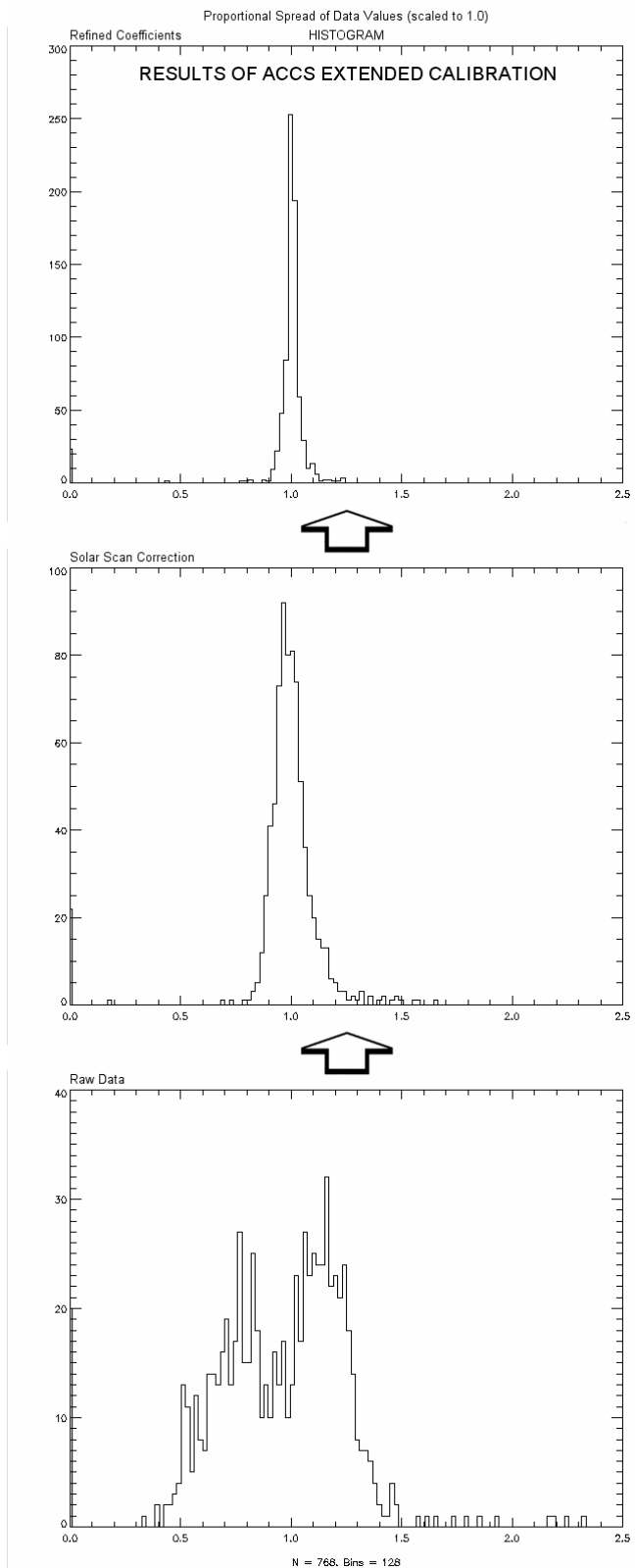
Figure 14. Efficacy of "fixed pattern" noise correction. The bottom panel shows the variability in a single wavelength without correction. The second panel shows how the variance is reduced after scanning solar cal while the top panel shows the final result. Note how variance is reduced by both steps.

4.   LESSONS LEARNED

1) The procurement process must be started as early as possible, using planning purchase requests if necessary. By using zero dollar planning purchase requests to start the long-lead purchasing process before funds were allocated, but after the instrument was approved for the mission, the LAC team was able to advance the contract award dates for items such as the detector arrays and the linear variable (wedged) filters by several months.

2) All subsystem elements should be subjected to internal, informal, independent peer reviews early in the design cycle. The LAC initially had particular problems obtaining a reliable, well-modeled design for one of the electronic boards (the digital board). An independent peer review identified several inherent design flaws, which were subsequently corrected. This allowed a robust working digital board to be fabricated. Several other lesser problems in other subsystems were also caught by good independent reviews.

3) Appropriate computer modeling tools should be used for all complex circuitry. One of the problems with the digital board design process was that the initial software used to model the behavior of the field programmable gate arrays (FPGAs) and the microcomputer on the digital board did not provide a high-fidelity representation of the behavior of the actual hardware. Thus, results from the model were not borne out by actual hardware tests. This meant that multiple FPGAs were irreversibly programmed and incorporated into what was supposed to be the flight version of the digital board. Since the models did not correctly predict the behavior of the board, this wasted time and money.

4) Instrument delivery schedules should be driven by a realistic assessment of the launch schedule, and not by sliding deadlines. The LAC was delivered approximately one year before shipment for launch. Much of this time could have been spent in better calibrating the instrument.

5) The number of formal, external reviews should be limited to one, or two at most. These reviews absorb resources in the form and time and money and rarely identify problems not already identified by the team. Conversely, informal contacts with knowledgeable outside reviewers should be encouraged.

6) The ability of an agile spacecraft to provide calibration opportunities not specifically planned before launch is an extremely valuable asset. These possibilities should be anticipated as much as possible during mission planning, so that calibration procedures can be improved. The LAC was able to use a nodding solar scan, a maneuver not planned before launch, to identify and correct a systematic noise source that apparently appeared after launch.

5.   CONTACT INFORMATION

Dr. Dennis C. Reuter
NASA/GSFC
Code 693 (Planetary Systems Branch)
Greenbelt, MD 20771
Phone: 301-286-2042
Fax: 301-286-0212
e-mail: dennis.c.reuter@gsfc.nasa.gov

Mr. George H. McCabe
NASA/GSFC and Catholic University of America
Code 693
Greenbelt MD 20771
Phone: 301-286-8283
Fax: 301-286-0212
e-mail: george.mccabe@gsfc.nasa.gov

6.   SUMMARY

The LAC on EO-1 has successfully demonstrated a wedged filter hyperspectral imager on a space-based platform. This technology is highly desirable because of its inherent mechanical, electrical, and optical simplicity, its low mass and its robust nature because of the total avoidance of moving parts. The two-module design allows a wide range of optical design possibilities to be accommodated by changing the lenses or filters and/or arrays in the optics module while keeping the interface and power functions unchanged in the electronics module. Conversely, different spacecraft command and data interface architectures may be accommodated by modifying the electronics module and leaving the optics module unchanged. Although, on first glance, the data produced by imagers of this type are unusual, the data system developed for EO-1 produces products identical to those produced by more conventional optical systems. Indeed, the wedged filter system may be used for any application requiring low to moderate spatial resolution hyperspectral imaging data, except for those with a rapid temporal variation (i.e., variability on a time scale shorter than that required to scan the spectrum). The wedged filter system is especially attractive for applications covering a wide wavelength range, but where only segments of the spectrum are needed. In this case, a single array may be used segmenting the wedge to cover only the spectral ranges desired.

The LAC has also demonstrated the utility of space based natural sources for calibration purposes. In future systems the solar calibration tubes will have calibrated off-axis performance characteristics, so that scanning solar calibrations may be used to provide absolute radiometric calibration as well as relative measures. Future atmospheric correctors will also employ InGaAs arrays whose lattice matching InP layers have been thinned to allow shorter wavelength operation. These arrays already exist and will allow operation throughout the visible spectral region, increasing the usefulness for aerosol monitoring.

6.1   Water Vapor Retrieval Example

Figure 15 illustrates the usefulness of the LAC in determining integrated vertical atmospheric water vapor abundances. The example shown here is for an area near Venice, Italy. The left panel shows a measure of the atmospheric transmittance as defined by the ratio $I(1.0945)/I(1.0425)$, where $I(\lambda)$ is the measured reflected intensity at wavelength λ. Since atmospheric water vapor absorbs radiation at 1.0945 μm, while 1.0425 μm is relatively free of water vapor absorption, this ratio is larger (approaching a maximum of 1) when the atmosphere is dry, while it decreases (approaching 0) as the water vapor increases. The wing of the band (1.0945 μm) is used rather than the band center at about 1.133 μm, because the band center is frequently saturated, decreasing sensitivity at this wavelength. The right panel shows an image of the scene at 1.0463 μm, another wavelength at which there is little water vapor absorption. This band is used for comparison rather than the image at 1.0425 μm used in the ratio, to avoid serendipitous correlations. Note that regions of clouds in the monochromatic image (bright) show up as regions of low water vapor (also bright) in the ratio image. This is because the reflecting clouds are at higher altitude than the surface and therefore there is less integrated water above the cloud layer than above the surface. Also note that the water vapor decreases in the areas of raised topography for a similar reason. This rough estimate will be improved upon with better modeling of the atmospheric water vapor band, but it already illustrates the usefulness of the approach.
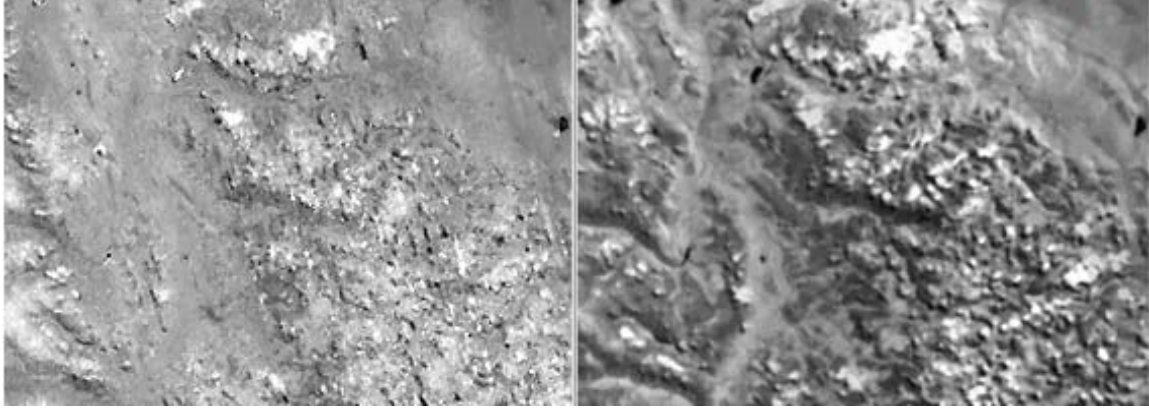
Figure 15. Comparison of retrieved water vapor (left panel) with monochromatic image in the 1.0463 μm relative window region. Regions of reduced atmospheric water vapor show up as brighter areas on the left. Note the bright spots in the top center of both images. This is a region of clouds, which show up as a reduced water vapor because the column path is reduced. Also note the expected lower water vapor amounts above regions of high topography.

7.   REFERENCES

[1] "The Highly Integrated Pluto Payload System (HIPPS): A Sciencecraft Instrument for the Pluto Mission. " S. A. Stern , D. C. Slater, W. Gibson, H. J. Reitsema, Alan Delamere, D. E. Jennings, D. C. Reuter, J. T. Clarke, C. C. Porco, E. M. Shoemaker and J. R. Spencer, *SPIE Proceedings, EUV, X-RAY and Gamma-Ray Instrumentation for Astronomy VI*, **2518**, 39 - 58, San Diego, CA; July 1995.

[2] "Logarithmically Variable Infrared Etalon Filters." K. P. Rosenberg, K. D. Hendrix, D. E. Jennings, D. C. Reuter, M. D. Jhabvala, and A. T. La, *SPIE Proceedings, Optical Thin Films IV: New Developments*, **2262**, 25 - 27 July, 1994, San Diego, CA.

[3] "Hyperspectral Sensing Using the Linear Etalon Imaging Spectral Array." D. C. Reuter, D. E. Jennings, G. H. McCabe, J. W. Travis, V. T. Bly, A. T. La, T. L. Nguyen, M. D. Jhabvala, P. K. Shu and R. D. Endres, *SPIE Proceedings of the European Symposium on Satellite Remote Sensing III: Conference on Sensors, Systems, and Next Generation Satellites II,* **2957**, 154-161, September 23-26, 1996, Taorima, Sicily, Italy.

[4] G. T. Elerding, J. G. Thunen and L. M. Woody. "Wedge Imaging Spectrometer: application to drug and pollution law enforcement." *SPIE Vol. 1479, Surveillance Technologies*, Orlando, FL; April 1991.

[5] L. M. Woody and J. C. Dermo. "Wedge Imaging Spectrometer (WIS) hyperspectral data collections demonstrate sensor utility." *International Symposium on Spectral Sensing Research (ISSR) 1994*, San Diego, CA; July 1994.

[6] "Observations Using the Airborne Linear Etalon Imaging Spectral Array (LEISA): A 1- to 2.5- micron Hyperspectral Imager for Remote Sensing Applications." G. McCabe, D. C. Reuter, SC. Tsay, P. L. Coronado, D. E. Jennings, P. K. Shu, P. Mantica, S. Cain, M. Abrams, Arthur L. Boright and J. L. Ross, *SPIE Proceedings of the European Symposium on Satellite Remote Sensing VI: Conference on Sensors, Systems, and Next Generation Satellites V,* September 20-24, 1999, Florence, It.

[7] Keifer, H. Private Communication, 2002.

ACRYONYMS and ABBREVIATIONS

2-D	Two-dimensional		LEISA	Linear Etalon Imaging Spectral Array
A/D	Analog-to-Digital		LUT	Look-up Table
AC	Atmospheric Corrector		LVE	Linear Variable Etalon
ACCS	Atmospheric Corrector Calibration System		Mbits/s	Megabits per second
ALI	Advanced Land Imager		mrad	milliradian
C&DH	Command and Data Handling		MS	Multispectral
cm	centimeter		N_2	Nitrogen
DCE	Data Collection Event		nm	nanometer
DPF	Data Processing Facility		NRA	NASA Research Announcement
EO	Earth Observing		PV	Photovoltaic
FOV	Field of View		s	second
GSFC	Goddard Space Flight Center		SNR	Signal-to-Noise Ratio
HS	Hyperspectral		SVF	Science Validation Facility
Hz	Hertz		TEC	Thermal Electric Cooler
I	Measured Reflected Intensity		USGS	U.S. Geologic Survey
InGaAs	Indium Gallium Arsenide		VNIR	Visible and Near-Infrared
InP	Indium Phosphide		W	watts
IR	Infrared		WFOV	Wide Field of View
K	Kelvin		WIS	Wedged Imaging Spectrometer
kg	kilogram		μm	micrometer
LAC	LEISA Atmospheric Corrector			